Interpretable AI for Liver Cancer Detection: Cascaded CNN & GLCM Integration

Bellary Chiterki Anil
Department of CSE (AI & ML), JSS Academy of Technical Education, Bengaluru, India
anilbc@jssateb.ac.in

Jayasimha Sondekoppa Rajkumar
Department of MCA, JSS Academy of Technical Education, Bengaluru, India
jayasimhasr@jssateb.ac.in (corresponding author)

Arun Kumar Gowdru
Department of E&CE, JSS Academy of Technical Education, Noida, Uttar Pradesh, India
arunkumargowdru.1981@gmail.com

Kiran P. Rakshitha
Department of MCA, Dayananda Sagar College of Engineering, Bangalore, India
rakshitha-mcavtu@dayanandasagar.edu

Samitha Khaiyum
Department of MCA, Dayananda Sagar College of Engineering, Bangalore, India
samitha-mcavtu@dayanandasagar.edu

Basavaiah Lathamani
Department of Management Studies, JSS Academy of Technical Education, Bengaluru, India
lathamanib@jssateb.ac.in

Balakrishnan Ramadoss
Department of Computer Applications, National Institute of Technology, Tiruchirappalli, Tamil Nadu, India
brama@nitt.edu

Received: 7 January 2025 | Revised: 27 January 2025 | Accepted: 1 February 2025

 DOI: https://doi.org/10.48084/etasr.10147

ABSTRACT

Liver cancer has significantly high mortality, especially in regions such as Africa and Asia. Early detection enhances treatment options, but indications are frequently not apparent until advanced stages. This research introduces an explainable AI (XAI) approach using a cascaded Convolutional Neural Network (CNN) combined with Gray Level Co-occurrence Matrix (GLCM)-based texture features to segregate non-cancerous from malicious tumors. The CLD system was used for assessment, and the approach was examined using the TCIA dataset, demonstrating higher accuracy and interpretability compared to prevailing techniques. XAI methods, such as feature importance and model visualization, were employed to provide details on the decision-making process of the model, ensuring transparency and reliability in clinical applications.

Keywords-Hepatocellular Carcinoma (HCC); Metastatic Carcinoma (MC); Convolutional Neural Network (CNN); Machine Learning (ML); Explainable Artificial Intelligence (XAI); Gray Level Cooccurrence Matrix (GLCM)

I. INTRODUCTION

Hepatocellular Carcinoma (HCC), is a malignant tumor that occurs as an outcome of the proliferation of cancer cells in the liver, causing serious problems due to high mortality and recurrence. Early and accurate identification of tumors with CT scan slices is important for good treatment planning and patient outcomes. This research focuses on the use of explainable Artificial Intelligence (XAI) technology to improve the clarity and definition of deep learning models developed for cancer diagnosis. The main goal is to identify malignant tissue (including the liver and adjacent organs) from CT scan slices to facilitate volumetric assessment and evaluation of cancer progression due to the need for sophisticated diagnostic tools that deliver not only high precision but also clear interpretations to aid clinical decision-making.

This study employs a cascaded CNN combined with GLCM texture features to segment and classify liver tumors. Additionally, XAI methods are incorporated to provide insights into the model execution procedure. This approach aims to enhance trust among medical practitioners by providing explanations for the results of the model, highlighting the significance of feature relevance, and visualizing the segmented regions. By integrating XAI techniques, this study not only seeks to achieve high diagnostic precision but also prioritizes the interpretability of the results, which is essential for clinical acceptance and effective treatment planning. Such techniques can ensure that the model decision-making procedure is transparent and interpretable, fostering trust and acceptance in clinical settings.

TABLE I. EXPLAINABLE AI (XAI) TECHNIQUES

Technique	Description	Application in Study
Feature Importance	Identifies and ranks the most significant features used by the model to make predictions.	Used to determine which GLCM features and CNN layers contribute most to the classification of cancer cells.
Model Visualization	Provides visual interpretations of how the model processes inputs and makes decisions.	Visualizes the regions of interest in CT scans that the CNN focuses on, helping to understand the areas that influence predictions.
SHAP (SHapley Additive exPlanations)	Calculates the contribution of each feature to the final prediction, offering a local explanation.	Applied to explain individual predictions by illustrating the influence of individual features on the model's result.
LIME (Local Interpretable Model-agnostic Explanations)	Creates interpretable models approximating the behavior of the complex model.	Used to explain specific predictions by approximating the complex CNN model with a simpler, interpretable model.
Saliency Maps	Highlights the pixels in the input image that most influence the model's output.	Generates heatmaps indicating the crucial areas of the CT scans that lead to classification decisions.

This study discusses various XAI methods, such as SHAP and LIME, which are applied to improve the interpretability of AI models in cancer classification, specifically for lung and colon cancer. In [1], the significance of transparency in AI models in building trust among clinicians and ensuring accurate diagnoses was highlighted. ML models integrated with XAI techniques can effectively predict liver cancer. Techniques such as SHAP and Grad CAM are employed to interpret the model predictions, making the decision-making process transparent and understandable for medical professionals [2]. This study surveyed XAI methods used in image classification, discussing the trade-offs between model accuracy and interpretability, and presenting a taxonomy of XAI methods and their applications in medical imaging, including liver cancer detection [3].

This study proposes a novel approach for diagnosing and predicting liver cancer using a Fully Cascaded CNN (FCNN). Unlike traditional methods that analyze image patches, this FCNN processes whole images, thus improving the efficiency and accuracy of segmentation and classification tasks [4]. The study highlights the importance of employing XAI techniques to make the model's predictions more transparent, which is crucial for gaining clinical trust. Additionally, it introduces an advanced version of Grad CAM, called Attention Guided Grad CAM, which enhances the interpretability of CNN models used in medical image classification [5]. This technique is especially effective in identifying key areas in liver cancer images, facilitating precise diagnosis. Furthermore, it explores how integrating GLCM with CNNs can improve the interpretability of liver cancer detection models, making the predictions more understandable for clinicians [6, 7].

In [7], a comprehensive review explored recent advancements in XAI within the healthcare sector, particularly in clinical settings. This article emphasized the importance of AI in creating transparent and reliable models for diagnosing and treating diseases such as cancer. LIME and SHAP offer visual explanations of model predictions to aid clinicians in decision-making processes [8]. This study compared various XAI approaches utilized in medical diagnostics, including cancer detection, assessing the benefits and drawbacks of each approach with an emphasis on improving model transparency and interpretability. Additionally, the study discusses different CNN methods integrated with XAI to advance cancer diagnosis, demonstrating how various tests and interpretative techniques can increase the accuracy and clarity of cancer diagnoses [9].

II. METHODOLOGY

Figure 1 illustrates a detailed workflow for analyzing and classifying CT images using a blend of advanced image processing and deep learning methods. The process starts with the acquisition of CT scan images, which are then enhanced through preprocessing to improve image quality. Subsequently, an initial segmentation is performed using a CNN that segments the image into various regions or structures of interest. This segmentation step is essential for isolating specific areas for further analysis. Subsequently, features are removed from segmented images using the GLCO method, which analyzes texture by examining the spatial relationships between pixels to identify patterns and structures within the CT images. These topographies are then entered into another CNN for classification, allowing the identification of specific structures, abnormalities, or other relevant features in the images. This two-stage CNN approach ensures both accurate segmentation and precise classification. The preliminary

segmentations are further refined using the Active Contour Method (ACM) and regression methods. ACM enhances object detection by evolving curves to align more precisely with the boundaries of structures in the images, while regression techniques are employed to fine-tune these initial results. The final stage incorporates XAI methods, namely saliency maps, Grad CAM, or SHAP, to construe and elucidate the results of the AI models. This step is crucial to verify model performance and ensure that the results are both reliable and interpretable. The lower part of the diagram displays the various stages of the CT image analysis workflow, illustrating the progression from raw data to the final classified and annotated images. Each stage signifies different levels of refinement and analysis applied to the CT images, emphasizing the detailed and cyclical nature of this process. In general, this approach integrates traditional image analysis techniques with contemporary deep learning methods to deliver a comprehensive and interpretable solution for CT image analysis.

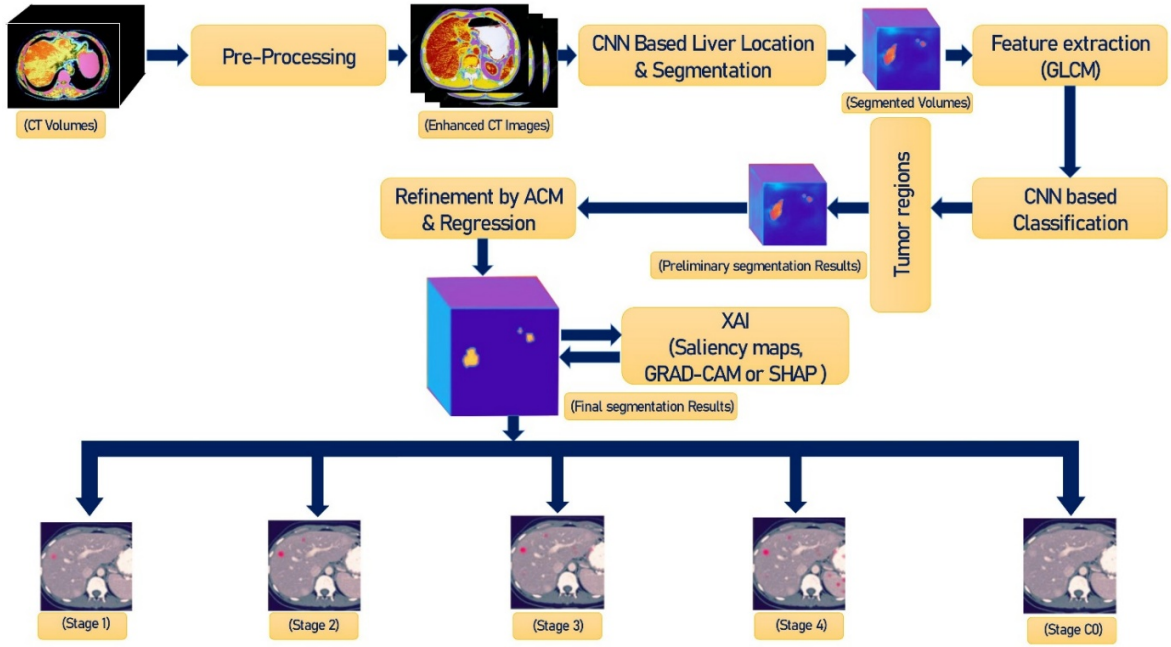

Fig. 1. The proposed method.

A. *Step 1: Preprocessing*

Preprocessing of CT scans involves several steps, such as converting images to grayscale and applying median filters. However, many of the latest automated deep learning methods are developed without considering preprocessing techniques, which may reduce their reliability, especially when handling larger datasets or extended periods. CT scan data typically contain various types of noise, including impulse noise, Gaussian noise, and quantization noise. To address these issues, the first step focuses on optimizing the intensity levels of low-contrast CT images, minimizing noise interference, and improving the performance of deep-learning models.

$$X = imadjust(Y) \quad (1)$$

$$X = imadjust(Y, [L_{in}, H_{in}]) \quad (2)$$

$$X = imadjust(Y, [L_{in}, H_{in}], [L_{out}, H_{out}]) \quad (3)$$

Equation (1) describes the remapping of the intensity levels to improve the contrast of the output image. The $imadjust()$ function enhances contrast by clipping the top and bottom by one percent of pixel intensity readings. Equation 2 uses L_{in} and H_{in} to represent the min and max input intensity readings, which are normalized on a scale between 0 and 1. Subsequently, (3) encompasses this by recording these normalized readings an $[L_{out}, H_{out}]$ range, effectively minimizing noise and reducing image relics.

B. *Step 2: Noise Reduction*

Noise reduction is applied to CT segment volumes and to isolate the liver region. This approach builds upon existing methods by utilizing a CNN for liver detection and segmentation while incorporating temporal phase transitions. Figure 2 illustrates how convolutional filters and neural network layers work together, playing a key role in achieving precise liver analysis. The tailored CNN architecture for 2D abdominal liver segmentation allows for accurate identification in liver regions. This process uses dual-layer classifiers to differentiate between liver and non-liver regions with softmax possibilities. This design consists of five layers, integrating input with multiple images, and incorporates fully connected networks and max pooling techniques to enhance feature extraction. The system employs ResNet as an encoder, a Global Convolutional Network (GCN) for decoding, and a PatchGAN as a classifier to achieve high-resolution segmentation. It was initially made as an axial slice and then converted to NIFTI format to create 3D volume in DICOM images. Every axial slice in the 3D CT was converted to 256×256 pixels for

training and testing. The following segment discusses how malicious tumors are identified by generating tumor candidates within the segmented regions, with Figure 2 showcasing the resulting segmentation [10].

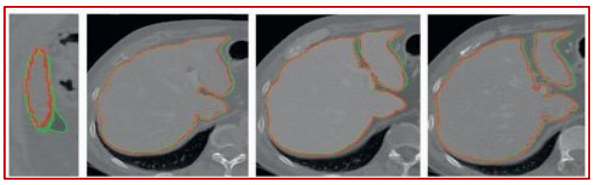

Fig. 2. Segmentation results: green outlines show manually identified boundaries, while red outlines indicate automated detection.

C. Step 3: Extract Region Of Interest (ROI)

A GLCM-CNN approach is used to effectively excerpt the ROI on the segmented liver. This procedure captures a dispersal of gray levels, representing pixel radiance readings, and gathers texture information by considering spatial relationships between pixel pairs at various angles and distances (e.g., 0º, 45º, 90º, 120º) [11]. The GLCM matrix is calculated based on the occurrence of these pixel pairs. Several properties of GLCM are used, such as energy (uniformity), homogeneousness (Inverse Difference Moment), and contrast.

$$H = \frac{\sum_{a,b=1}^{X} M_{a,b}}{1+(a+b)^2} \quad (4)$$

$$E = \sum_{a,b=1}^{X} M_{a,b^2} \quad (5)$$

$$C = \sum_{a,b=1}^{X} M_{a,b}\,(a-b)^2 \quad (6)$$

These GLCM texture features are unified into the input layer of the CNN to improve classification accuracy. The architecture begins with a 228×344 pixel image derived from GLCM features. Additional features, such as the major and minor axis lengths, perimeter, and area, are also calculated to enhance the model's performance.

$$E = \frac{a}{b} \quad (7)$$

$$P = (P_{a,b}, A_{edge}[P] = a, B_{edge}[P] = b) \quad (8)$$

$$A = (A_{a,b}, A_{ROI}[Area] = a, B_{ROI}[Area] = b) \quad (9)$$

The GLCM CNN architecture consists of convolutional subsampling and output layers. The subsampling function averages the values in the input patch window:

$$A_j = \frac{avg}{n*n}\left(A_j^{n*n} * X(n,n)\right) \quad (10)$$

The output layer, linked to the final convolutional layer, contains four to five neurons corresponding to different cancer stages. CNN training aims to reduce the mean squared error defined in (11) [12], using a training data sample X that represents the total number of samples in training, a class target $d_j(n)$, a batch number B, an output from the j^{th} layer $y_j(n)$, and a normalized squared error $E_{average}$.

$$E_{average} = \frac{1}{X}\sum_{a=1}^{B}(d_j\,(n) - y_j(n))^2 \quad (11)$$

D. Step 4: Liver Tumor Identification Refinement

ACM is used to refine liver tumor identification. This model involves contour initiation, regional formulation, and boundary formulation to fine-tune tumor identification. The region function evaluates the exterior and interior regions, while the function u assigns a reading between 0 and 1 to every pixel of x.

$$min_{0\le u\le 1}\left(\int_{\Omega} g_b|\nabla u|dx + \lambda\int_{\Omega} h_r u dx\right) \quad (12)$$

E. Step 5: XAI

After refining the liver tumor identification using ACM, the results are processed using XAI techniques. XAI enhances the interpretability of the GLCM-CNN model's outputs by providing intuitions into the executive process. One approach involves using SHAP values, which quantify each feature's influence on the model's predictions. The SHAP value for a feature i is specified by:

$$\varphi_i = \sum S \subseteq \frac{N}{\{i\}\left(\frac{|S|!(|N|-|S|-1)!}{|N|!}\right)}\left(f(S\cup\{i\} - f(S)\right) \quad (13)$$

where S represents a subset of features, N denotes the complete set of features, and f refers to the prediction function of the model. This calculation helps to understand which features, such as homogeneity, energy, contrast, and perimeter, are most influential in classifying the stages of cancer. Additionally, the LIME was employed to create locally interpretable approximations of the model's predictions. LIME perturbs the input data and observes vicissitudes in the predictions to build an interpretable model around each one. The weight $w(z)$ of a perturbed instance z in the local neighborhood is defined as:

$$w(z) = exp(-\text{distance}(z, z')^2/2\sigma^2 \quad (14)$$

where z' is the instance being explained, and σ controls the size of the neighborhood. LIME generates explanations for individual predictions, highlighting how specific features affect the model's output. This phase not only confirms the reliability and transparency of the proposed GLCM-CNN model but also builds trust in the results among medical professionals.

F. Dataset

This study used CT scan images sourced from The Cancer Imaging Archive (TCIA), a publicly available medical imaging database. A total of 137 cases with annotated liver cancer CT scans were selected, covering both cancerous and non-cancerous instances. To prepare the data for analysis, preprocessing steps, such as intensity normalization, noise reduction, and resizing, were applied to standardize the images to 256×256 pixels. CT slices were organized into 3D nifti volumes to facilitate segmentation and classification tasks. This dataset was selected due to its high-quality annotations and diverse representation of liver cancer cases, allowing the effective validation of the proposed method [13-15]. The dataset was split into 80:20 for training (110 cases) and testing (27 cases). The model achieved a training dice coefficient of 84.8 ± 13.5% and a testing accuracy of 82.6 ± 13.9%. SHAP and LIME were applied to enhance model interpretability and clinical transparency.

III. RESULTS AND DISCUSSION

This study thoroughly compared and assessed a range of segmentation methods against the proposed approach, integrating XAI to enhance interpretability. Through scrupulous study and assessment with other methods [15, 16], XAI enabled us to elucidate the proposed segmentation approach, which significantly outperformed the other methods, showing a prominent enhancement in dice precision of 6-11%. Classification accuracy was calculated using:

$$A = \frac{number\ of\ correct\ identifications}{total\ number\ of\ data} \times 100 \qquad (15)$$

Accuracy computation methods can differ [17]. For an in-depth understanding, it is proposed to consult the original studies for detailed accuracy calculations. Table II provides the range of values, including the highest and lowest, for each tumor classification. With the incorporation of XAI, these outcomes are augmented by enhanced interpretability and model transparency. Deprived of detailed data, however, precise scores and assessments for every metric cannot be provided [18]. Figures 3 and 4 provide a quantitative assessment of the proposed segmentation method, comparing its performance against both CNN and GLCM-CNN techniques. Using an XAI-driven model, GLCM-CNN provides better accuracy, underscoring the benefits of interpretability in model performance evaluation.

Table III provides a comprehensive assessment of the proposed XAI approach to analyze segmentation outcomes for tumors of varying sizes: large, medium, and small. Evaluation employed metrics such as the maximum symmetric surface distance, the average symmetric surface distance, the relative volume differences, the volume overlap error, and the dice coefficient per case to measure performance [19, 20]. This table allows for a detailed examination of the results and provides critical insights into the effectiveness of the proposed procedure with different tumor sizes [21].

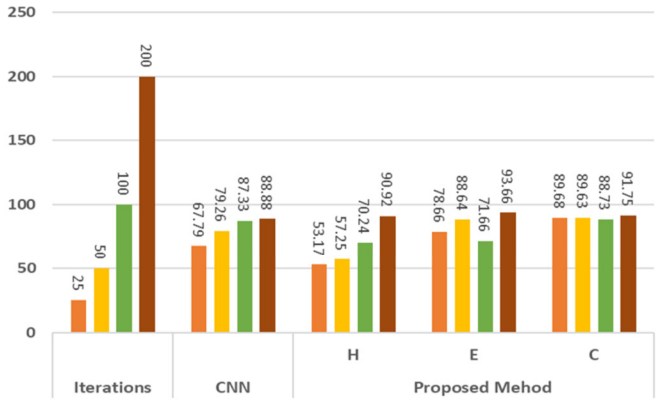

Fig. 3. Graphical representation of classification accuracy of CNN and GLCM-CNN.

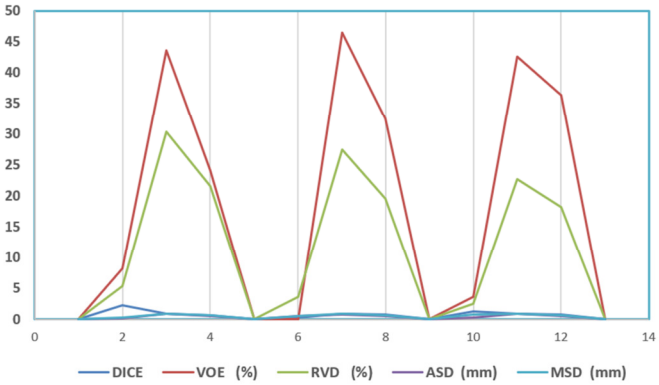

Fig. 4. Graphical illustration of scores (Table III).

TABLE II. EVALUATION OF THE PROPOSED TUMOR SEGMENTATION TECHNIQUE

	DICE	**VOE (%)**	**RVD (%)**	**ASD (mm)**	**MSD (mm)**
Small tumor	0.89 ± 2.25	37.91 ± 8.26	27.69 ± 5.36	0.78 ± 0.21	0.97 ± 0.30
Max	0.89	43.66	30.32	0.93	0.93
Min	0.72	24.13	21.62	0.55	0.70
Medium	0.83 ± 0.25	39.62 ± 9.62.	24.54 ± 3.72	0.75 ± 0.51	1.15 ± 0.52
Max	0.92	46.53	27.56	0.85	0.86
Min	0.74	32.46	19.63	0.57	0.68
Large tumor	0.92 ± 1.25	38.95 ± 3.62	19.23 ± 2.56	0.78 ± 0.32	1.12 ± 0.84
Max	0.95	42.54	22.80	0.93	0.87
Min	0.77	36.32	18.23	0.52	0.67
Average	0.89 ± 7.08	29.05 ± 5.32	24.25 ± 2.96	0.78 ± 0.56	1.12 ± 0.21

TABLE III. CLASSIFICATION ACCURACY OF THE PROPOSED XAI METHOD

Iterations	**CNN**	**Proposed method**		
		H	**E**	**C**
25	67.79	53.17	78.66	89.68
50	79.26	57.25	88.64	89.63
100	87.33	70.24	71.66	88.73
200	88.88	90.92	93.66	91.75

IV. CONCLUSION

This study presented a novel cascaded approach for liver cancer detection, combining CNN with GLCM texture features to improve diagnostic accuracy. This approach addressed the gap between model performance and interpretability by integrating XAI techniques, such as SHAP and LIME, to provide clear insights into the model's decision-making process. Unlike existing methods, the proposed approach

refined segmentation using ACM and employed detailed preprocessing steps tailored for CT scan data, resulting in superior dice similarity coefficients and improved classification performance. Focusing on interpretability and transparency not only advances diagnostic accuracy but also lays a foundation for greater clinical trust and adoption of AI in liver cancer diagnostics. This process achieved better results, with a dice similarity coefficient of 84.8 ± 13.5% for training and 82.6 ± 13.9% for testing on CT images of 137 patients. The addition of XAI methods enhances the model's reliability by providing clear and interpretable insights into its operations, further supporting its potential clinical adoption.

This research uniquely integrates radiomic-driven texture analysis with deep learning to improve liver cancer detection. The application of XAI methods ensures that the decision-making process is transparent and interpretable, addressing a key limitation in AI-driven medical diagnostics. Furthermore, the refined segmentation approach using ACM enhances the accuracy of lesion localization, contributing to improved classification results. The proposed approach significantly advances liver cancer diagnostics by providing a highly accurate, interpretable, and clinically reliable AI model. By leveraging radiomics, deep learning, and XAI, this study not only improves classification performance but also enhances trust in AI-based diagnostics. The combination of these elements lays the foundation for potential real-world clinical adoption, bridging the gap between advanced computational techniques and practical medical applications.

REFERENCES

[1] M. B. Moin, F. T. J. Faria, S. Saha, B. K. Rafa, and M. S. Alam, "Exploring Explainable AI Techniques for Improved Interpretability in Lung and Colon Cancer Classification." arXiv, May 14, 2024, https://doi.org/10.48550/arXiv.2405.04610.

[2] C. Bouron *et al.*, "Prognostic Value of Metabolic, Volumetric and Textural Parameters of Baseline [18F]FDG PET/CT in Early Triple-Negative Breast Cancer," *Cancers*, vol. 14, no. 3, Jan. 2022, Art. no. 637, https://doi.org/10.3390/cancers14030637.

[3] G. S. Sannala, K. V. G. Rohith, A. G. Vyas, and C. R. Kavitha, "Explainable Artificial Intelligence-Based Disease Prediction with Symptoms Using Machine Learning Models," in *IoT Based Control Networks and Intelligent Systems*, vol. 789, P. P. Joby, M. S. Alencar, and P. Falkowski-Gilski, Eds. Singapore: Springer Nature Singapore, 2024, pp. 523–538.

[4] A. Chaddad, J. Peng, J. Xu, and A. Bouridane, "Survey of Explainable AI Techniques in Healthcare," *Sensors*, vol. 23, no. 2, Jan. 2023, Art. no. 634, https://doi.org/10.3390/s23020634.

[5] Y. Abas Mohamed, B. E. Khoo, M. Shahrimie Mohd Asaari, M. Ezane Aziz, and F. Rahiman Ghazali, "Decoding the black box: Explainable AI (XAI) for cancer diagnosis, prognosis, and treatment planning-A state-of-the art systematic review," *International Journal of Medical Informatics*, vol. 193, Jan. 2025, Art. no. 105689, https://doi.org/10.1016/j.ijmedinf.2024.105689.

[6] P. Barra, A. Della Greca, I. Amaro, A. Tortora, and M. Staffa, "A Comparative Analysis of XAI Techniques for Medical Imaging: Challenges and Opportunities," in *2024 IEEE International Conference on Bioinformatics and Biomedicine (BIBM)*, Lisbon, Portugal, Dec. 2024, pp. 6782–6788, https://doi.org/10.1109/BIBM62325.2024.10821983.

[7] O. Sarkar *et al.*, "Multi-Scale CNN: An Explainable AI-Integrated Unique Deep Learning Framework for Lung-Affected Disease Classification," *Technologies*, vol. 11, no. 5, Sep. 2023, Art. no. 134, https://doi.org/10.3390/technologies11050134.

[8] B. C. Anil and P. Dayananda, "Automatic Liver Tumor Segmentation based on Multi-level Deep Convolutional Networks and Fractal Residual Network," *IETE Journal of Research*, vol. 69, no. 4, pp. 1925–1933, May 2023, https://doi.org/10.1080/03772063.2021.1878066.

[9] N. P. Nelaturi, V. Rajesh, and I. Syed, "Real-Time Liver Tumor Detection with a Multi-Class Ensemble Deep Learning Framework," *Engineering, Technology & Applied Science Research*, vol. 14, no. 5, pp. 16103–16108, Oct. 2024, https://doi.org/10.48084/etasr.8106.

[10] N. C. Kundur, B. C. Anil, P. M. Dhulavvagol, R. Ganiger, and B. Ramadoss, "Pneumonia Detection in Chest X-Rays using Transfer Learning and TPUs," *Engineering, Technology & Applied Science Research*, vol. 13, no. 5, pp. 11878–11883, Oct. 2023, https://doi.org/10.48084/etasr.6335.

[11] M. Kass, A. Witkin, and D. Terzopoulos, "Snakes: Active contour models," *International Journal of Computer Vision*, vol. 1, no. 4, pp. 321–331, Jan. 1988, https://doi.org/10.1007/BF00133570.

[12] P. F. Christ *et al.*, "Automatic Liver and Tumor Segmentation of CT and MRI Volumes using Cascaded Fully Convolutional Neural Networks." arXiv, Feb. 23, 2017, https://doi.org/10.48550/arXiv.1702.05970.

[13] Y. Yuan, "Hierarchical Convolutional-Deconvolutional Neural Networks for Automatic Liver and Tumor Segmentation." arXiv, Oct. 12, 2017, https://doi.org/10.48550/arXiv.1710.04540.

[14] A. L. Simpson *et al.*, "Preoperative CT and survival data for patients undergoing resection of colorectal liver metastases," *Scientific Data*, vol. 11, no. 1, Feb. 2024, Art. no. 172, https://doi.org/10.1038/s41597-024-02981-2.

[15] K. Clark *et al.*, "The Cancer Imaging Archive (TCIA): Maintaining and Operating a Public Information Repository," *Journal of Digital Imaging*, vol. 26, no. 6, pp. 1045–1057, Dec. 2013, https://doi.org/10.1007/s10278-013-9622-7.

[16] G. Chlebus, H. Meine, J. H. Moltz, and A. Schenk, "Neural Network-Based Automatic Liver Tumor Segmentation With Random Forest-Based Candidate Filtering." arXiv, Jun. 27, 2017, https://doi.org/10.48550/arXiv.1706.00842.

[17] X. Han, "Automatic Liver Lesion Segmentation Using A Deep Convolutional Neural Network Method," *Medical Physics*, vol. 44, no. 4, pp. 1408–1419, Apr. 2017, https://doi.org/10.1002/mp.12155.

[18] K. He, X. Zhang, S. Ren, and J. Sun, "Deep Residual Learning for Image Recognition," in *2016 IEEE Conference on Computer Vision and Pattern Recognition (CVPR)*, Las Vegas, NV, USA, Jun. 2016, pp. 770–778, https://doi.org/10.1109/CVPR.2016.90.

[19] C. Peng, X. Zhang, G. Yu, G. Luo, and J. Sun, "Large Kernel Matters — Improve Semantic Segmentation by Global Convolutional Network," in *2017 IEEE Conference on Computer Vision and Pattern Recognition (CVPR)*, Honolulu, HI, Jul. 2017, pp. 1743–1751, https://doi.org/10.1109/CVPR.2017.189.

[20] P. Isola, J. Y. Zhu, T. Zhou, and A. A. Efros, "Image-to-Image Translation with Conditional Adversarial Networks," in *2017 IEEE Conference on Computer Vision and Pattern Recognition (CVPR)*, Honolulu, HI, Jul. 2017, pp. 5967–5976, https://doi.org/10.1109/CVPR.2017.632.

[21] S. Saha Roy, S. Roy, P. Mukherjee, and A. Halder Roy, "An automated liver tumour segmentation and classification model by deep learning based approaches," *Computer Methods in Biomechanics and Biomedical Engineering: Imaging & Visualization*, vol. 11, no. 3, pp. 638–650, May 2023, https://doi.org/10.1080/21681163.2022.2099300.